Eur. Phys. J. D **46**, 59–67 (2008)
DOI: 10.1140/epjd/e2007-00287-1

THE EUROPEAN PHYSICAL JOURNAL D

Multiphoton ionization of iodine atoms and CF_3I molecules by XeCl laser radiation

V.N. Lokhman, D.D. Ogurok, and E.A. Ryabov[a]

Institute of Spectroscopy, Russian Academy of Sciences, 142190 Troitsk, Moscow region, Russia

Received 9 June 2007
Published online 12 October 2007 –

Abstract. We report about effective ionization of iodine atoms and CF_3I molecules under the action of intense XeCl laser radiation (308 nm). The only ion fragment resulting from the irradiation of the CF_3I molecules is the I^+ ion. We have studied the influence of the intensity, spectral composition, and polarization of the laser radiation used on the intensity of the ion signal and the shape of its time-of-flight peak. Based on the analysis of the results obtained, we have suggested the mechanism of this effect. The conclusion drawn is that the ionization of the iodine atoms by the ordinary XeCl laser with a nonselective cavity results from a three- $(2 + 1)$-photon REMPI process. This process is in turn due to the presence of accidental two-photon resonances between various spectral components of the laser radiation and the corresponding intermediate excited states of the iodine atom. The probability of ionization of the atoms from their ground state $I(^2P_{3/2})$ by the radiation of the ordinary XeCl laser is more than two orders of magnitude higher than the probability of their ionization from the metastable state $I^*(^2P_{1/2})$. The ionization of the CF_3I molecules by the XeCl laser radiation occurs as a result of a four-photon process involving the preliminary one-photon dissociation of these molecules and the subsequent $(2 + 1)$-photon REMPI of the resultant neutral iodine atoms.

PACS. 32.80.Rm Multiphoton ionization and excitation to highly excited states – 33.80.Rv Multiphoton ionization and excitation to highly excited states – 42.55.Lt Gas lasers including excimer and metal-vapor lasers

1 Introduction

The multiphoton ionization (MPI) of atoms, molecules, and radicals, their resonance-enhanced multiphoton ionization (REMPI) included, is being widely used to detect these particles and to study their highly excited states and also chemical reactions involving them (see, e.g. [1,2], as well as the reviews [3,4]). Based on this technique, the spectral properties of the CF_3I molecule and the photoinduced reactions occurring during the course of excitation of its various states have been investigated in fairly great detail. For example, using the REMPI method to detect iodine atoms, the authors of [5,6] have studied the unimolecular decay of CF_3I as a result of its IR multiphoton excitation within the limits of the ground electronic term (see Fig. 1). The decay products in that case are the CF_3 radical and the iodine atom in the ground state $^2P_{3/2}$. The above authors used the $(3 + 1)$-photon REMPI of atomic iodine by radiation in the visible region of the spectrum. It should be noted that the $(2 + 1)$-photon REMPI of iodine by radiation in the ultraviolet region [7,8] proved more convenient and sensitive. The first excited electronic state of the CF_3I molecule (A band, begins at approximately 32 000 cm^{-1}) is a decaying one and has a fairly complex structure. It is formed by three potential surfaces, $^3Q_1$, $^3Q_0$, and $^1Q_1$, two of them ($^3Q_0$ and $^1Q_1$) intersecting (see Fig. 1). This in turn makes the picture of decay from this state rather involved. The dissociation of the molecule subsequent upon excitation of its $A \leftarrow X$ transition is accompanied by the prompt fission of the C–I bond (according to the data of [9], the lifetime amounts to 150–350 fs), two reaction channels being active to produce iodine atoms in the ground, $I(^2P_{3/2})$, and the excited, $I^*(^2P_{1/2})$, state:

$$CF_3I + h\nu \rightarrow CF_3 + I(^2P_{3/2}), \quad (1)$$

$$CF_3I + h\nu \rightarrow CF_3 + I^*(^2P_{1/2}). \quad (2)$$

Reactions (1) and (2) and the effect of the crossing between the $^3Q_0$ and $^1Q_1$ states on them have been studied in a series of works (see, e.g., [10,11] and references cited therein). Specifically, the $(2 + 1)$ REMPI detection of atomic iodine was used, in conjunction with the velocity map imaging technique [11], too, to determine the I^*/I branching ratio and the photofragmentation anisotropy parameters β for reactions (1) and (2) and also the dependence of these parameters on the radiation wavelength

[a] e-mail: ryabov@isan.troitsk.ru

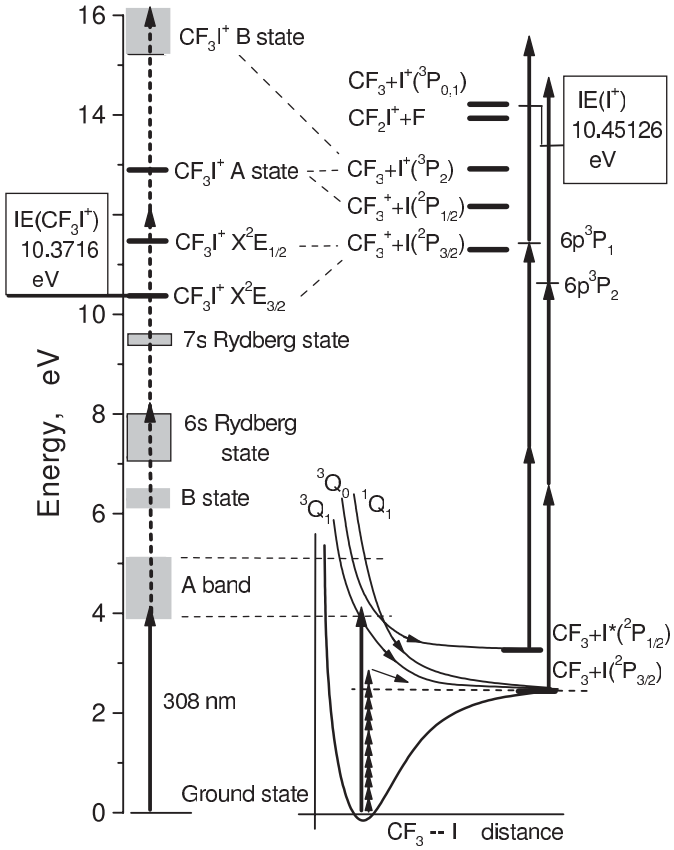

Fig. 1. Left: energy level diagram of the CF_3I molecule and CF_3I^+ ion. Right and bottom: the A and X states of the CF_3I molecule and schematic diagrams of its UV and IR MP excitation, along with the schematic diagram of the $(2+1)$ REMPI of atomic iodine.

and the vibrational excitation extent of CF_3. Note that the I*/I branching ratio also depends on the temperature (vibrational) of the CF_3I molecules themselves, and when the latter are excited at $\lambda = 308$ nm, it increases with the temperature [12].

The REMPI technique was also used to study high-lying electronic states of both the CF_3I molecule itself and the molecular ion CF_3I^+. To illustrate, the (2+1) REMPI by laser radiation tunable within the range 300–306 nm was used in [13] to investigate the 6s Rydberg manifold (C state, Fig. 1). Observed in the mass spectrum of the ionization products were the CF_3I^+, CF_3^+ and I^+ ions. The photofragmentation of the CF_3I^+ ion produced by way of the (2+1) REMPI process in the range 300–306 nm was also studied in [14]. In that case, as distinct from [13], there also occurred an intermediate resonance with the decaying A term of the CF_3I molecule. Nevertheless, the ion contents of the products observed were the same. The authors of [13,14] concluded that the CF_3I^+ ion resulted from the $(2+1)$-photon resonant ionization of CF_3I. The emergence of the other two ions, as well as the relation between the CF_3I^+, CF_3^+, and I^+ ion peaks, largely depends on the possibility of absorption of a fourth photon by the CF_3I^+ ion, followed by its dissociation into $CF_3^+ + I$ or $CF_3 + I^+$. Besides, some CF_3^+ ions may be produced via the statistical dissociation of the source CF_3I^+. This conclusion about the formation mechanism of the ion products was supported by the results of the later work [15]. What is more, the conclusion was drawn in this work that the direct four-photon excitation of the parent molecule prior to its ionization was unlikely with nanosecond lasers. It should be noted that high-lying states in CF_3I^+ were also studied using the one-photon ionization of CF_3I by VUV radiation (see, e.g., [16]). The results obtained correlate well with those obtained by the REMPI method.

The advent of femtosecond lasers has allowed the dynamics of photoinduced reactions to be studied directly. In particular, such investigations into the dynamics of the multiphoton dissociation and ionization of CF_3I were carried out in [17,18]. By varying the delay between the pump and probe pulses made it possible to reveal, among other things, the sequence and emergence time of the ion fragments. This time proved to differ between different fragments, which is explained by the competition between different ion production pathways. Thus, the above brief overview demonstrates that sufficiently detailed information have been obtained to date about the structure of the electronic states in CF_3I and CF_3I^+, as well as on the channels and energies of photoinduced reactions in these particles. It was these data, presented in [5–18], that were used in preparing Figure 1.

In all of the above-cited works, to ionize the CF_3I molecule, use is made of intermediate resonance states, as a rule, from the 6s or the 7s Rydberg manifold. As a result, the ionization spectrum features a distinct structure determined mainly by the vibronic states of the intermediate resonances. When the ionizing radiation is detuned off resonance with these states, the ion signal vanishes. In our experiments with the CF_3I molecule we have found that the ionization of the CF_3I molecule under the effect of XeCl laser radiation (308 nm) occurs at a radiation intensity over some 1.6×10^8 W/cm^2. But in contrast to the above-mentioned experiments, the resultant mass spectrum in our experiments contained only one ion product, namely, the iodine ion, I^+. No other products, be it CF_3I^+ or CF_3^+, have been found. What is more, XeCl laser radiation has been found to be even more effective in ionizing atomic iodine, predominantly from its ground state $^2P_{3/2}$. To reveal the mechanism governing the ionization of iodine atoms and CF_3I molecules by the XeCl laser radiation, we have conducted special investigations. The results of this work are presented in this paper.

2 Experimental

We performed our experiments using the setup whose detailed description can be found in [19,20]. This experimental setup allows one to take measurements with both molecular beams and low-pressure (10^{-7}–10^{-8} Pa) gases at room temperature (298 K). It was precisely this, second regime that was used in our experiments with CF_3I, whose results are presented in this paper. The atomic iodine needed for the experiments was produced by way of the IR

multiphoton dissociation (IR MPD) of CF_3I by a pulsed CO_2 laser radiation (duration 150 ns, line 9R12) resonant with the ν_1 mode of this molecule. The energy fluence of the CO_2 laser radiation used amounted to 8 J/cm^2, which ensures almost 100% dissociation of CF_3I to yield iodine atoms in the ground state $^2P_{3/2}$ state (see, e.g., [21]). The CF_3I gas was irradiated directly within the chamber of a home-built time-of-flight mass spectrometer (TOF MS) used to detect and identify the ion fragments formed. The focused XeCl and CO_2 laser beams propagated at an angle of 60° to each other in a plane normal to the axis of the TOF MS, so that their caustic waists intersected on this axis. The XeCl laser beam was focused by means of a lens with a focal length of $f = 12$ cm, the focal spot diameter of the beam (at the $1/e$ level) amounted to 0.13 mm. The CO_2 laser beam at this spot was 1 mm in diameter.

It is well-known [22] that the structure of the emission spectrum of the ordinary XeCl laser in the 308-nm region is conditioned by the vibrational-rotational structure of its radiative transitions. The strongest among them are the transitions $\nu'' = 1 \leftarrow \nu' = 0$ and $\nu'' = 2 \leftarrow \nu' = 0$, emitting radiation with a wavelength (in air) of 307.961 and 308.21 nm, respectively. To narrow the spectrum of our XeCl laser and enable one to select the necessary transition, the laser cavity was modified as in [23]. Instead of the nontransparent mirror, use was made of a grating (2400 lines/mm) set at a grazing incidence angle. In addition, the cavity was equipped with two diaphragms 11 mm in diameter. All this made it possible to sufficiently effectively control the radiation spectrum (see below). The radiation of our modified XeCl laser was linearly polarized, normal to the axis of the TOF MS. The "ordinary" spectrum was not polarized. In that case, linear polarization was attained, if need be, by means of a Glan prism.

The ions formed inside the chamber of the TOF MS were detected with a secondary-electron multiplier. The ion signal, as well as the UV and IR pulse energies, were monitored by a digital oscilloscope and then fed to a computer to be accumulated and processed. A triggering circuit was used to time all the pulses.

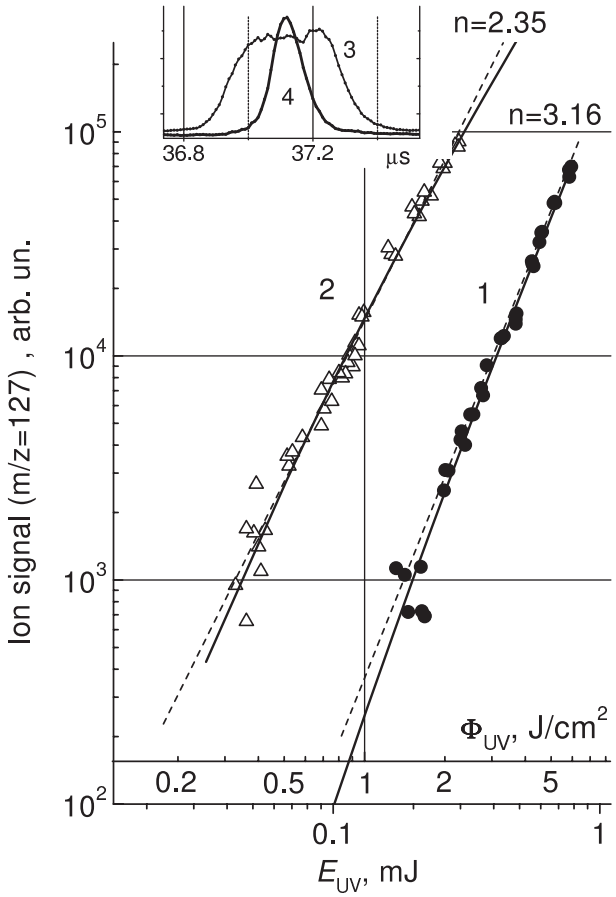

Fig. 2. Yield of the I^+ ions as a function of the XeCl laser pulse energy (fluence) in the multiphoton ionization of CF_3I (curve 1) and atomic iodine (curve 2). Symbols – experimental points, dotted lines – approximation by a power function, solid curves – model calculations. Φ_{UV} – fluence values in the center of UV beam spot. CO_2 laser fluence used to produce iodine atoms, $\Phi_{IR} = 7.7$ J/cm^2. Arbitrary units – same for both curves 1 and 2. Inset: characteristic shape of the time-of-flight peaks of the I^+ ions in the ionization of CF_3I (curve 3) and atomic iodine (curve 4).

3 Results and discussion

As noted above, in our experiments with the CF_3I molecule, we found that irradiating it with a sufficiently intense XeCl laser radiation made the molecule undergo ionization to produce the I^+ ion peak in the mass spectrum. Figure 2 presents the relationship measured between the magnitude of the ion signal $S(I^+)$ and the laser pulse energy (curve 1). The data points in the initial section of this curve correspond to a radiation intensity around 1.5×10^8 W/cm^2. One can see that the experimental data points fit well the power dependence $S(I^+) \propto E_{UV}^n$ (dashed curve) close to a cubic one: the power $n = 3.16$. Note that no other ions, be it CF_3^+ or CF_3I^+, were found when irradiating the CF_3I molecule in the XeCl laser radiation intensity range studied.

When the CF_3I molecules were preliminarily made to dissociate into CF_3 and $I(^2P_{3/2})$ as a result of their IR MPD under the effect of a CO_2 laser pulse, the mass spectrum resulting from their irradiation with the XeCl laser also featured the I^+ ion peak, which undoubtedly evidenced the ionization of iodine atoms by this radiation. Curve 2 in Figure 2 represents the relationship between $S(I^+)$ and E_{UV} at a CO_2 laser radiation energy fluence of $\Phi_{IR} = 7.7$ J/cm^2. The delay between the IR and UV pulses amounted to 1.2 μs. Under these conditions, by the instant the UV pulse arrived, practically 100% of the CF_3I molecules had already undergone dissociation, and the recession of the iodine atoms formed could still be disregarded [21]. As can be seen from Figure 2, the behavior of the $S(I^+)$ signal in this case differs noticeably from that in the case of irradiation of the CF_3I molecules (cf. curves 1 and 2). When ionizing iodine, the experimental dependence of the ion signal on the energy fluence E_{UV} is also described by a power function, but it is now closer to the quadratic function $S(I^+) \propto E_{UV}^n$ ($n = 2.36$)

shown by the dashed line superimposed on curve 2. Besides, since the number of particles, the iodine atoms I and the CF_3I molecules, in both cases is approximately the same, it appears from Figure 2 that the process of ionization of the iodine atoms is more effective than that of the CF_3I molecules (cf. curves 1 and 2). It should be noted that the time-of-flight spectra of the I^+ ions differ between these two cases as well. The corresponding peaks are presented in the inset in Figure 2. The width of the peak in the case of ionization of the CF_3I molecules is obviously much greater than in the case of ionization of the iodine atoms. This in turn points to the fact that the kinetic energy of the I^+ ions formed in the former case is perceptibly higher than in the latter. The time-of-flight spectra will be considered in more detail elsewhere.

Thus, the above results allow us to conclude that the formation of the I^+ ions during the course of irradiation of the CF_3I molecules and the iodine atoms, I, occurs as a result of multiphoton processes, but the actual formation mechanism differs between these two cases.

3.1 Multiphoton ionization of iodine atoms

As already noted, the (2 + 1) REMPI of atomic iodine was studied in a series of works. There are two resonances in the region of 308 nm that correspond to two-photon transitions from the ground state $5p^2P_{3/2}$ ($5p^2P_{3/2} \rightarrow 6p^3P_2$) and from the excited state $5p^2P_{1/2}$ ($5p^2P_{1/2} \rightarrow 6p^3P_1$) to the appropriate intermediate levels in iodine. The laser radiation frequency needed to excite these transitions equals 32 451.73 cm^{-1} and 32 463.16 cm^{-1}, respectively [8]. Recall that the frequencies of the 0–1 and 0–2 transitions in the XeCl laser are (as reckoned from the positions of the radiation intensity maxima) 32 462.2 cm^{-1} and 32 436 cm^{-1}, respectively. At first glance it would seem that the closest to resonance with the XeCl laser radiation is the transition in the excited iodine I^* that in our experiments can be produced by reaction (2). However, as follows from the experiment (see Fig. 2), the ionization of iodine from its ground state is much more effective.

We have measured the actual spectrum of the 0–1 and 0–2 transitions in our XeCl laser. When the laser uses a nonselective cavity, the spectrum is as shown in Figure 3a. One can see that both transitions are of finite width, and the profile itself features a substructure associated with the rotational components of the vibronic transitions. With the spread function of our spectral instrument known ($\Delta_{(1/2)} = 2$ cm^{-1}), we could deconvolve this instrumental width and obtain a model spectrum of our XeCl laser. This model spectrum is also presented as the shaded profile in Figure 3a. The spectrum shows the possible position of the individual rotational components of the transitions. Note that the rotational structure of the model spectrum obtained is in good agreement with the well-known direct measurement results, at least for the $\nu'' = 1 \leftarrow \nu' = 0$ transition. Specifically, the distances obtained by us between the lines of this transition (Fig. 3a) agree well with the values obtained in [24] for the states with $j' = 4$, 5, 6, 7, and 8. Note that the spectrum of

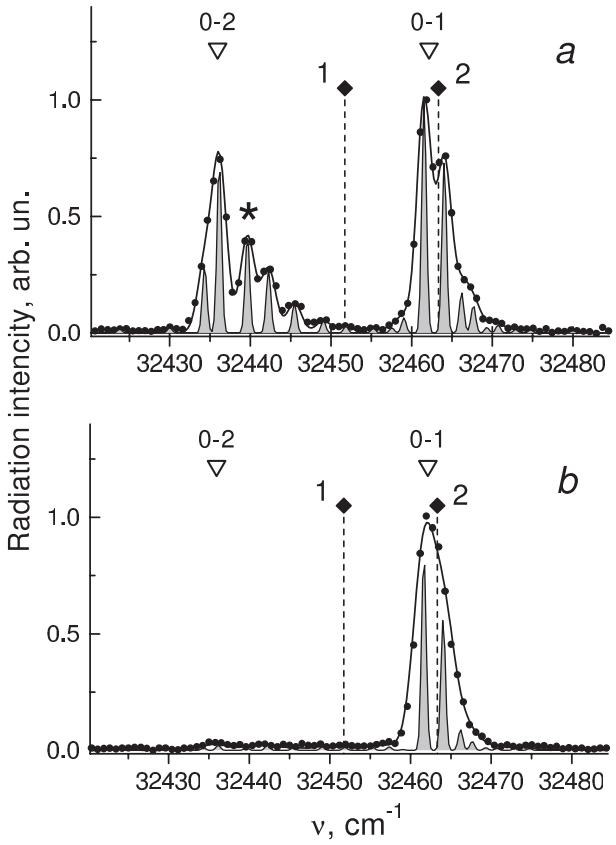

Fig. 3. Fragment of the XeCl laser emission spectrum. Symbols (∇) indicate the position of the maxima of the 0–1 and 0–2 transitions. Symbols (♦) and dashed lines indicate the position of the nearest two-photon resonances for $I(^2P_{3/2})$ and $I^*(^2P_{1/2})$, 1 and 2, respectively. The asterisk indicates the position of the maximum used to determine the parameter η (see text). (a) Nonselective cavity. Dots and solid curve – experiment; shaded profile – model spectrum, $\eta = 2.3$. (b) Selective cavity. The 0–2 transition is suppressed, $\eta = 37$.

Figure 3a only gives an idea of the position of the transition lines; unfortunately, their width remains undetermined, but it does not exceed 0.66 cm^{-1}. Indicated in Figure 3a are also the frequencies corresponding to two-photon transitions in I and I^*. The frequency needed to excite $I(^2P_{3/2})$ is seen to fall approximately midway between the frequencies of the 0–1 and 0–2 transitions. Therefore, the two-photon excitation of $I(^2P_{3/2})$ can become possible if one photon is taken from the 0–1 transition and the other, from the 0–2 one. By and large, for the probability of two-photon excitation of a state with an energy of $h\nu$, we may write

$$S(\nu) \propto \iint d\nu_1 d\nu_2 I(\nu_1) I(\nu_2) \delta(\nu_1 + \nu_2 - \nu)$$
$$= \int d\nu_1 I(\nu_1) I(\nu - \nu_1) = (I * I)(\nu), \qquad (3)$$

where $I(\nu)$ is the spectral density distribution of the XeCl laser radiation. Expression (3) is actually the convolution of the model spectrum presented in Figure 3a. The result

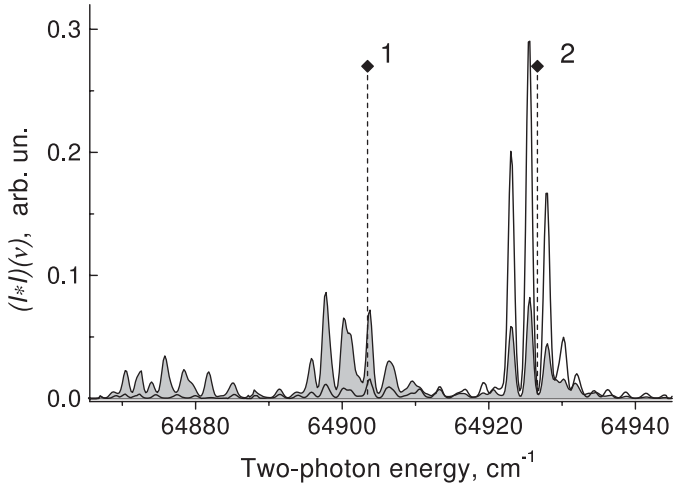

Fig. 4. Convolution of the model spectrum of the XeCl laser. Shaded profile – nonselective cavity, $\eta = 2.3$. Open profile – selective cavity, $\eta = 37$. 1 and 2 – two-photon transition energies for $I(^2P_{3/2})$ and $I^*(^2P_{1/2})$, respectively.

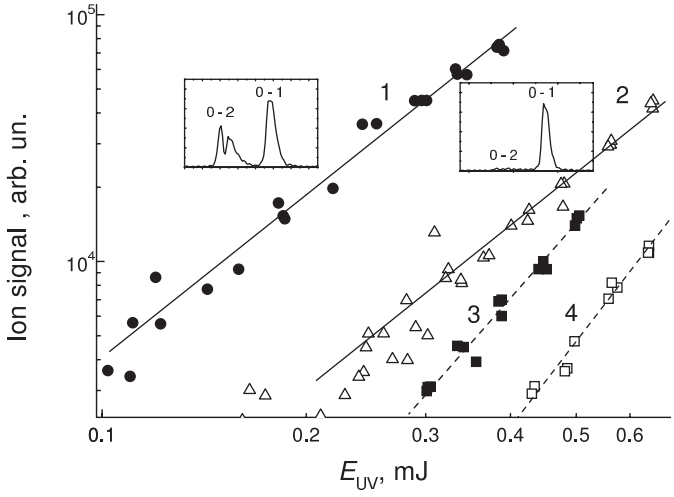

Fig. 5. Effect of the spectral composition of the XeCl laser radiation on the ionization efficiency of iodine atoms (curves 1 and 2) and CF_3I molecules (curves 3 and 4). Presented are the dependences of $S(I^+)$ on E_{UV} for nonselective cavity ($\eta = 2.3$, curves 1 and 3) and for selective cavity ($\eta = 37$, curves 2 and 4). Arbitrary units – same for all the curves.

of this convolution of the model spectrum of our XeCl laser radiation is presented in Figure 4. One can clearly see that the effective excitation of $I(^2P_{3/2})$ is indeed possible, whereas the two-photon resonance for $I^*(^2P_{1/2})$ occurs in the spectral minimum. To verify this conclusion, we measured the ionization yield for the modified spectrum. Using a selective cavity, we varied the relation between the intensities of the 0–1 and 0–2 transitions. A characteristic example of such a spectrum, with the 0–2 transition largely suppressed, is shown in Figure 3b. The relation between the intensities of the 0–1 and 0–2 transitions was characterized by the parameter $\eta = a/b$, the ratio of the amplitude of the 0–1 transition to the maximum amplitude denoted by the asterisk (*) on the spectrum of the 0–2 transition (Fig. 3a). For the usual spectrum of our XeCl laser with a nonselective cavity the ratio $\eta = 2.3$, and for the spectrum of Figure 3b, $\eta = 37$.

We also measured the yield $S(I^+)$ of the I^* iodine as a function of the *total* UV pulse energy E_{UV} for various η values. Curve 2 in Figure 5 represents the relationship between $S(I^+)$ and E_{UV} for $\eta = 37$. The same figure also shows for comparison a similar relationship (curve 1) measured under the same conditions for the usual spectrum, i.e., for $\eta_0 = 2.3$. It can be seen that reducing η by a factor of 16 leads to a 7.8-fold reduction of the ion signal. Similar relationships were also measured for other η values. As a result, we obtained the dependence of the normalized signal $S_n = S(\eta)/S(\eta_0)$, where $\eta_0 = 2.3$, on the parameter η, the total energy E remaining the same. This dependence is represented by triangles in Figure 6. We can demonstrate that within the framework of the assumptions made, including the one that $a + b = \text{const.}$,

$$S_n = \frac{\dfrac{\eta}{(1+\eta)^2}}{\dfrac{\eta_0}{(1+\eta_0)^2}}.$$

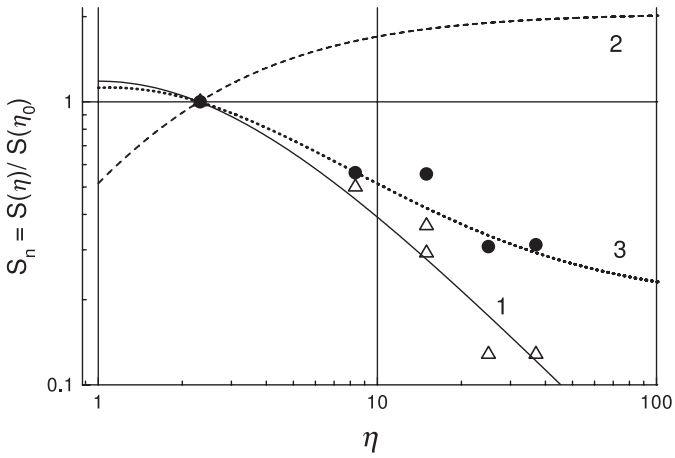

Fig. 6. Normalized ion signal $S_n = S(\eta)/S(\eta)$ as a function of the parameter η – the ratio between the intensities of the 0–1 and 0–2 XeCl laser transitions (see text). Triangles and curve 1 – experiment and calculation for the ionization of $I(^2P_{3/2})$; dashed curve 2 – calculation for the ionization of $I^*(^2P_{1/2})$; circles and dotted curve – experiment and calculation for the ionization of CF_3I. Polarization – normal to the axis of the TOF MS.

A graphic idea of this dependence can be gained from curve 1 of Figure 6. A sufficiently good agreement with the experiment is obvious.

We believe that the results presented give grounds to state that the ionization of $I(^2P_{3/2})$ by the XeCl laser radiation results from the simultaneous utilization of two different photons from the 0–1 and 0–2 transitions. The absorption of a third photon by the atom raises it into the ionization continuum. Thus, we have to do here with the three- $(2 + 1)$ REMPI of the $I(^2P_{3/2})$ atom by the XeCl laser radiation, resulting from the accidental resonance of

the sum of the energies of two different photons from the 0–1 and 0–2 transitions in this laser with the energy of the $5p^2P_{3/2} \rightarrow 6p^3P_2$ transition in the iodine atom. As for the deviation of the observed dependence $S(I^+) \propto E_{UV}^{2.36}$ from the cubic behavior expected to occur in this case, it is apparently due to the saturation of the transition from the intermediate state $6p^3P_2$ into the ionization continuum. The modeling of this type of (2 + 1) process in a rate equations approach and in a wide range of fluences including saturation region makes it possible to determine the cross-section σ_i of above ionization transition (see, e.g. [2]). The result of this modeling is shown in Figure 2 by the solid curve drawn via the experimental points (2). A good agreement between the measured and calculated data is seen. This fitting procedure gave the magnitude of σ_i equal to 2.3×10^{-18} cm^2. This value falls into the characteristic region of 10^{-17}–10^{-18} cm^2 for the ionization cross-section of atoms from their excited states [2]. The measured σ_i value corresponds to the saturation energy $\Phi_s = h\nu/2\sigma_i = 1.4$ J/cm^2. The curve (2) in Figure 2 is measured at $\Phi_{UV} \approx 0.45$–2.3 J/cm^2 so that saturation (at least partial) of this transition in our experiments should be really seen.

Note in conclusion that the (2 + 1) REMPI of the $I(^2P_{3/2})$ atoms by the XeCl laser radiation makes it possible to determine the mean velocity of these atoms during the course of dissociation of the CF_3I molecules. This can be done by measuring the recession kinetics of the particles as a function of the delay between the IR and UV pulses (for details, see [25]), and also proceeding from the width of the time-of-flight peak of these atoms. In both cases, for $\Phi_{IR} \approx 4$ J/cm^2, we obtained closely similar mean velocity values, around 270 m/s. Considering the initial thermal velocity of the CF_3I molecules, this gives 0.088 eV for the kinetic energy release ε in the IR MPD of CF_3I by reaction (1).

3.2 Multiphoton ionization of CF_3I molecules

There are two possible ways for the I^+ ions to form during the course of irradiation of the CF_3I molecules by the XeCl laser radiation. The first is the direct multiphoton ionization of these molecules. The minimum energy required to produce the iodine ion by the reaction $CF_3I \rightarrow e^- + CF_3 + I^+(^3P_2)$ comes to 12.78 eV [15], and so three quanta at a wavelength of 308 nm prove insufficient for this reaction to be realized. To produce the I^+ ion requires absorption of at least four such photons, which is supported by the data of [13–15], already noted in the introduction. At the same time, as follows from these works, the formation of the iodine ion in that case is always accompanied by the emergence of the CF_3I^+ and CF_3^+ ions. And we emphasize once more that the only ion product formed in our experiment is the I^+ ion. Moreover, the ionization of CF_3I in [13–15] was only observed when the radiation frequency used was in a two-photon resonance with intermediate Rydberg state levels (see Fig. 1). As follows from the form of the spectrum of these transitions in the region of 300–306 nm [14], such a resonance in the vicinity of 308 nm is little probable. All this allows us to conclude that more probable is another way for I^+ to form, namely, as a result of the one-photon excitation of CF_3I into the state A, followed by the formation of the iodine atoms by reactions (1) and (2) and subsequent ionization of these atoms as a result of the (2 + 1) REMPI process considered above.

To reveal the mechanism of ionization of CF_3I by the XeCl laser radiation, we studied the effect of the spectral composition of this radiation (the relation between the 0–1 and 0–2 transitions) on the yield of the I^+ ions. The measurement results for the usual spectrum ($\eta_0 = 2.3$) and for the spectrum with $\eta = 37$ are presented in Figure 6 (curves 3 and 4, respectively). Similar relationships between $S(I^+)$ and the total energy E_{UV} were also measured for other η values. The magnitudes of the normalized ion signal $S_n = S(\eta)/S(\eta_0)$ obtained for various values of the parameter η are represented by circles in Figure 6. It can be seen that the behavior of S_n as a function of η is qualitatively similar to that in the case of the (2 + 1)-photon REMPI of the $I(^2P_{3/2})$ atoms. At the same time, the reduction of the ion signal with increasing η in the case of CF_3I takes its course obviously slower, especially at high η values. It should be noted that as distinct from the IR MPD of CF_3I, wherein only the $I(^2P_{3/2})$ atoms are produced, the UV dissociation of this molecule yields both $I(^2P_{3/2})$ and the excited iodine $I^*(^2P_{1/2})$. We, therefore, supposed that the slower reduction of S_n as a function of η (curve 3 in Fig. 6) is due to the REMPI of $I^*(^2P_{1/2})$ by the XeCl laser radiation within the limits of the 0–1 band. The spectrum in Figure 3a is a model spectrum; its fine structure is not resolved, and so the ionization of I^* is quite possible. If the probability of the two-photon excitation of $I^*(^2P_{1/2})$ is proportional to a^2, one can easily show that the relationship between the normalized ion signal $S_n = S(\eta)/S(\eta_0)$ and η for the excited iodine has the form

$$S_n = \frac{\dfrac{\eta^2}{(1+\eta)^2}}{\dfrac{\eta_0^2}{(1+\eta_0)^2}},$$

which is reflected by curve 2 of Figure 6. As expected, the magnitude of S_n grows higher with increasing η.

Within the framework of the assumptions made, we can write down the following expression for the total ion signal from the two iodine atom modifications: $S(I^+) \propto n_1\sigma_1^{(2)} 2ab\Phi_{UV}^2 + n_2\sigma_2^{(2)} a^2\Phi_{UV}^2$, where n_1 and n_2 are the partial concentrations and $\sigma_1^{(2)}$ and $\sigma_2^{(2)}$, two-photon transition cross-sections for I and I*, respectively. Finally, for the normalized total ion signal, we have

$$S_n = \frac{\dfrac{\eta}{(1+\eta)^2}}{\dfrac{\eta_0}{(1+\eta_0)^2}} \frac{1 + \dfrac{n_2\sigma_2^{(2)}}{2n_1\sigma_1^{(2)}}\eta}{1 + \dfrac{n_2\sigma_2^{(2)}}{2n_1\sigma_1^{(2)}}\eta_0}. \qquad (4)$$

The only unknown parameter in expression (4) is the ratio $n_2\sigma_2^{(2)}/n_1\sigma_1^{(2)}$. The best possible fit of expression (4) and

experimental data points is shown in Figure 6 by dashed curve 3. The value of the $n_2\sigma_2^{(2)}/n_1\sigma_1^{(2)}$ ratio corresponding to this case equals 0.09. Good agreement is evident between the experimental data points and curve (4), which confirms, in our opinion, the assumption made as to the formation mechanism of the I^+ ions. According to the data presented in [12], the relative concentration of I^* in the case of dissociation of CF_3I by the XeCl laser radiation at room temperature should be no less than 92%, i.e., $n_2 \geqslant 0.92$. Hence it follows that $\sigma_1^{(2)}/\sigma_2^{(2)} \geqslant 127$. This circumstance provides for a sufficiently high selectivity of ionization of the I atoms in their mixture with I^* by the XeCl laser radiation. Indeed, the ratio between the signals from I and I^* is $S(I)/S(I^*) = 2n_1\sigma_1^{(2)}/n_2\sigma_2^{(2)}\eta$, and at $n_1 = n_2$ and $\eta = 2.3$, we have $S(I)/S(I^*) \geqslant 110$.

We also conducted experiments and analyzed the time-of-flight spectra obtained with differing polarization of the exciting radiation. As noted earlier, the ion peak obtained after the preliminary IR MPD of CF_3I is substantially narrower than in the case of the UV irradiation of the source molecules (see Fig. 2). Moreover, as expected, the shape of this peak in the former case is, as expected, independent of the polarization of the exciting radiation. The characteristic shape of the time-of-flight signal from I^+ in the case of irradiation of CF_3I by the XeCl laser radiation is presented in Figures 7a and 7b for two polarization directions, normal and parallel to the z-axis of the TOF MS, respectively, and the "natural" spectrum of the radiation. These figures clearly demonstrate the anisotropy of the process of formation of I^+. We believe that both the shape of the ion peak and its width are determined by the first stage of the process, namely, the excitation and subsequent dissociation of CF_3I from the state $A \leftarrow X$ in accordance with reactions (1) and (2). This process has been studied well enough, including the case of $\lambda = 308$ nm [12]. The average translational energy release in the dissociation from the state A substantially exceeds that in the IR MPD within the X state. For example, in the case of excitation to the surface $^3Q_1 \leftarrow X$, the average velocity of the $I(^2P_{3/2})$ atoms formed is $V_m = 900$ m/s [12] (compare with the velocity $V_m = 270$ m/s measured by us in the IR MPD). It is exactly this fact that explains the materially greater width of the ion peak in the case of UV irradiation of CF_3I.

The shape of the time-of-flight peak in Figures 7a and 7b is governed by the distribution of the projections of the velocity V_z of the atoms produced onto the z-axis of the TOF MS. In analyzing our results, we used for this distribution the following expression similar to the one used in [26]:

$$P(V_z) = \int_{V_z}^{\infty} dV \left(\frac{P(V)}{2V} \left[1 + \beta P_2 \left(\frac{V_z}{V} \right) a \right] \right), \qquad (5)$$

where β is the anisotropy parameter, P_2 is a second-degree Legendre polynomial, and the parameter $a = 1$ or $a = -1/2$ for the polarization direction $\mathbf{E} \,||\, Oz$ or $\mathbf{E} \perp Oz$, respectively. As follows from [12], the transition

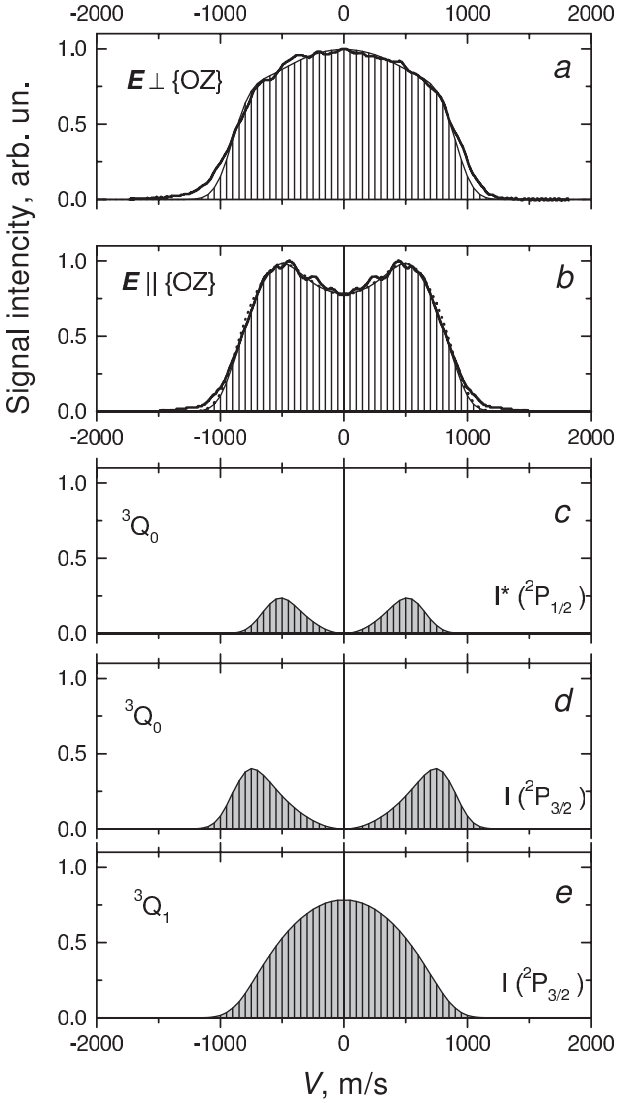

Fig. 7. Effect of the radiation polarization on the shape of the time-of-flight peak of I^+ produced upon irradiation of CF_3I – upper figures (a) and (b). The time-of-flight signal is presented in the velocity coordinate frame, where V – velocity projection onto z-axis of the TOF MS. (a) Experiment and calculation (shaded profile) for the case of polarization normal to the TOF MS axis; (b) experiment and calculation (shaded profile) for the case of polarization parallel to the TOF MS axis; (c–e) – calculated shape of the velocity distribution of iodine atoms for the different CF_3I dissociation channels (see text) and radiation polarization parallel to the TOF MS axis.

$^3Q_1 \leftarrow X$ is of perpendicular type, and for $\lambda = 308$ nm the parameter $\beta = -0.9$, while $^3Q_0 \leftarrow X$ is a parallel-type transition and, accordingly, $\beta = +1.8$ here. The velocity distributions $P(V)$ of the I atoms formed upon excitation of CF_3I onto these two surfaces differ in form. For $\lambda = 308$ nm, the form of $P(V)$ was determined in [12]. We used these data, taking into consideration the fact that the CF_3I molecules in our measurements were distributed by the initial room-temperature velocity distribution. When modeling the time-of-flight signal, account was also taken of the fact that the $I^*(^2P_{1/2})$ atoms were

only formed upon dissociation from the state $^3Q_0$, while the production of $I(^2P_{3/2})$ was contributed to not only by the state $^3Q_1$, but also by $^3Q_0$ (see Fig. 1). Figures 7c–7e present the shape of the velocity distribution of iodine atoms for each of these channels with the radiation polarization parallel to the z-axis of the TOF MS ($\mathbf{E} \,||\, Oz$). These distributions were used to calculate the shape of the overall time-of-flight signal. The best possible fit of the experimental signal and the sum of the contributions from the three channels is illustrated in Figure 7a (shaded profile). A similar procedure was also performed for $\mathbf{E} \perp Oz$ (Fig. 7a). In both cases, good agreement between the experiment and calculation is obvious. It should be noted that during the course fitting we also determined the relative contribution from each of the three atomic iodine formation channels to the total ion signal. The integral contribution to the ion signal from $I^*(^2P_{1/2})$ amounts to 0.122, that from $I(^2P_{1/2})$ formed as a result of the parallel and the perpendicular transition being equal to 0.254 and 0.624, respectively. (The data shown in Figs. 7c–7e are represented with these weights.) Hence it follows that the ratio between the signals from I and I^*, $S(I)/S(I^*)$, equals to 7.2. On the other hand, it has been demonstrated above that $S(I)/S(I^*) = 2n_1\sigma_1^{(2)}/n_2\sigma_2^{(2)}\eta$. For the measured value $2n_1\sigma_1^{(2)}/n_2\sigma_2^{(2)}\eta = 0.09$ and $\eta = 2.3$, we have $S(I)/S(I^*) = 9.66$. So, within the framework of the mechanism suggested for the production of the I^+ ions by the XeCl laser irradiation of the CF_3I molecules, two different types of experiment yield close values for the parameter $S(I)/S(I^*)$. This is another evidence in favor of this mechanism.

Thus, we believe that the set of the results presented allow us to quite justifiably state that when irradiating CF_3I by the XeCl laser radiation, I^+ ion emerges as a result of a four-photon process. At the first stage there takes place the one-photon dissociation of CF_3I to yield atomic iodine. The I^+ ions are then produced in the subsequent three- $(2+1)$-photon REMPI of these atoms as a result of accidental two-photon resonance between the XeCl laser radiation and the appropriate atomic transitions, the iodine atoms being predominantly ionized from their ground state $^2P_{3/2}$. As for the form of the power dependence of the ion signal $S(I^+)$ on the laser pulse energy E_{UV}, it should be noted that under our experimental conditions the transition $A \leftarrow X$ is not saturated. Indeed, according to [12], the cross-section of this transition is $\sigma = 3 \times 10^{-20}$ cm^2, and correspondingly, the saturation energy is $\Phi_s = h\nu/2\sigma \approx 11$ J/cm^2, and we took our measurements in the energy fluence range $1.6 - 6.4$ J/cm^2. For this reason, the power of the $S(I^+)$ dependence on E_{UV} should be approximately a unity greater than that for the subsequent REMPI process, which agrees well with the experiment (see Fig. 2). The difference of this dependence from a quartic one is caused again by the saturation of the transition to ionization continuum. The dependence of $S(I^+)$ on Φ_{UV} calculated within this approach with the measured earlier value of σ_i is presented in Figure 2 by the solid line (1). A good agreement with experiment is seen.

4 Conclusions

In this work, we report observation of the ionization of iodine atoms and CF_3I molecules under the effect of the XeCl laser radiation. When irradiating the molecules, the only ion product observed was the I^+ ion, which is distinct from the results obtained by other authors in a closely similar wavelength range, who always observed a number of different ions, including CF_3I^+, CF_3^+, and I^+. We measured the yield of the I^+ ions as a function of the XeCl laser radiation intensity and spectral composition and determined the effect of polarization of the radiation on the shape of the time-of-flight peak. The latter measurements showed the process of formation of I^+ upon the XeCl-laser irradiation of CF_3I to be anisotropic.

Our analysis of the results obtained has demonstrated that the main factor governing the possibility of effective ionization of the I atoms and CF_3I molecules is the finite width of the emission spectrum of the ordinary XeCl laser with a nonselective cavity, associated with the vibrational-rotational structure of the lasing band. We have concluded that the ionization of atomic iodine occurs as a result of a three- $(2+1)$ REMPI process. For the iodine atoms in the ground state $^2P_{3/2}$, this process takes place as a result of accidental resonance between the sum of the energies of two different photons from the 0–1 and 0–2 XeCl laser transitions with the energy of the $5p^2P_{3/2} \rightarrow 6p^3P_2$ transition in the iodine atom. The subsequent ionization of the atom from its state $6p^3P_2$ occurs as a result of absorption of a third photon. The ionization of the iodine atom from its metastable state $I^*(^2P_{1/2})$ also takes place as a result of a similar (2+1)-photon process, but in this case because of accidental resonance of the $5p^2P_{1/2} \rightarrow 6p^3P_1$ transition with two photons, both from the $0 \rightarrow 1$ XeCl laser emission band now. However, the probability of ionization of $I(^2P_{3/2})$ by the ordinary XeCl laser radiation proved to be much higher (by more than two, orders of magnitude) than that of $I^*(^2P_{1/2})$.

The results of our studies into the ionization of the CF_3I molecules by the XeCl laser radiation have allowed us to conclude that I^+ in that case is produced as a result of a four-photon process. The most probable mechanism responsible for this process is as follows. At the first stage there takes place the one-photon dissociation of CF_3I to produce neutral iodine atoms. The I^+ ions result from the subsequent three- $(2+1)$-photon REMPI of these atoms, the anisotropy of the entire process being determined by the first absorption stage.

We would like to note in conclusion that the ionization of atomic iodine by the XeCl laser radiation could be used as a convenient and effective means to detect iodine atoms in the ground state (by virtue of the high selectivity of this process), specifically in studying chemical reactions involving these atoms.

The authors would like to thank Prof. V.S. Letokhov for helpful discussions and Dr. V.M. Apatin for assistance in reconstruction of XeCl laser. This work was funded in part by Russian Foundation for Basic Research (Grant No. 07-02-00165) and

the Russian Academy of Sciences within the program "Optical Spectroscopy and Frequency Standards".

References

1. H. Reisler, C. Wittig, *Photodissociation and Photoionization*, edited by K.P. Lawley (John Wiley, Chichester, 1985), p. 1
2. V.S. Letokhov, *Laser Photoionization Spectroscopy* (Academic Press, Orlando, 1987)
3. M.N.R. Ashfold, J.D. Howe, Annu. Rev. Phys. Chem. **45**, 57 (1994)
4. K.V.D. Ledingham, R.P. Singhal, Int. J. Mass Spectr. Ion. Proc. **163**, 149 (1997)
5. P.A. Hackett, P. John, M. Mayhew, D.M. Rayner, Chem. Phys. Lett. **96**, 139 (1983)
6. V.N. Bagratashvili, S.I. Ionov, G.V. Mishakov, V. Semchishen, Chem. Phys. Lett. **115**, 144 (1985)
7. A. Gedanken, M.B. Robin, Y. Yafet, J. Chem. Phys. **76**, 4798 (1982)
8. J.-J. Jung, Y.S. Kim, W.K. Kang, K.-H. Jung, J. Chem. Phys. **107**, 7187 (1997)
9. Y.S. Kim, W.K. Kang, K.-H. Jung, J. Chem. Phys. **105**, 551 (1996)
10. A. Furlan, T. Gejo, J.R. Huber, J. Phys. Chem. **100**, 7956 (1996)
11. F. Aguirre, S.T. Pratt, J. Chem. Phys. **118**, 1175 (2003)
12. P. Felder, Chem. Phys. Lett. **197**, 425 (1992)
13. C.A. Taatjes, J.W.G. Mastenbroek, G. van den Hoek, J.G. Snijders, S. Stolte, J. Chem. Phys. **98**, 4355 (1993)
14. L.D. Waits, R.J. Horwitz, R.G. Daniel, J.A. Guest, J.R. Appling, J. Chem. Phys. **97**, 7263 (1992)
15. F. Aguirre, S.T. Pratt, J. Chem. Phys. **118**, 6318 (2003)
16. P. Downie, I. Powis, Faraday Discuss. **115**, 103 (2000)
17. W.G. Roeterdink, M.H.M. Janssen, Chem. Phys. Lett. **345**, 72 (2001)
18. H.P. Liu, Z.G. Sun, S.D. Hogan, N.Q. Lou, Eur. Phys. J. D **40**, 357 (2006)
19. A.V. Dem'yanenko, V.N. Lokhman, D.D. Ogurok, E.A. Ryabov, V.S. Letokhov, Chem. Phys. Lett. **320,** 594 (2000)
20. V.N. Lokhman, D.D. Ogurok, E.A. Ryabov, Tech. Phys. **50**, 846 (2005)
21. V.N. Bagratashvili, V.S. Letokhov, A.A. Makarov, E.A. Ryabov, *Multiple Photon Infrared Laser Photophysics and Photochemistry* (Harwood Acad. Pub., Chur, London, 1985)
22. J. Tellinghuisen, J.M. Hoffman, G.C. Tisone, A.K. Hays, J. Chem. Phys. **64**, 2484 (1976)
23. R. Buffa, P. Burlamacchi, R. Salimbeni, M. Matera, J. Phys. D: Appl. Phys. **16**, L125 (1983)
24. Q.-H. Lou, Hyp. Int. **38**, 531 (1987)
25. V.N. Lokhman, D.D. Ogurok, V.S. Letokhov, E.A. Ryabov, Z. Phys. Chem. **215**, 1469 (2001)
26. X. Chen, R. Maron, S. Rosenwaks, I. Bar, T. Einfeld, C. Maul, K.-H. Gericke, J. Chem. Phys. **114**, 9033 (2001)